J Appl Physiol
88: 1551–1557, 2000.

Fractal nature of regional ventilation distribution

WILLIAM A. ALTEMEIER,[1] STEVE MCKINNEY,[1] AND ROBB W. GLENNY[1,2]
University of Washington, Departments of [1]Medicine and [2]Physiology and Biophysics, Seattle, Washington, 98195-6522

Altemeier, William A., Steve McKinney, and Robb W. Glenny. Fractal nature of regional ventilation distribution. *J Appl Physiol* 88: 1551–1557, 2000.—High-resolution measurements of pulmonary perfusion reveal substantial spatial heterogeneity that is fractally distributed. This observation led to the hypothesis that the vascular tree is the principal determinant of regional blood flow. Recent studies using aerosol deposition show similar ventilation heterogeneity that is closely correlated with perfusion. We hypothesize that ventilation has fractal characteristics similar to blood flow. We measured regional ventilation and perfusion with aerosolized and injected fluorescent microspheres in six anesthetized, mechanically ventilated pigs in both prone and supine postures. Adjacent regions were clustered into progressively larger groups. Coefficients of variation were calculated for each cluster size to determine fractal dimensions. At the smallest size lung piece, local ventilation and perfusion are highly correlated, with no significant difference between ventilation and perfusion heterogeneity. On average, the fractal dimension of ventilation is 1.16 in the prone posture and 1.09 in the supine posture. Ventilation has fractal properties similar to perfusion. Efficient gas exchange is preserved, despite ventilation and perfusion heterogeneity, through close correlation. One potential explanation is the similar geometry of bronchial and vascular structures.

gas exchange; lung airway; lung mechanics

THE PRINCIPAL FUNCTION OF the lung is to exchange oxygen and carbon dioxide between blood and inspired air and is dependent on local matching of regional ventilation-to-perfusion ratio ($\dot{V}_A/\dot{Q}$). Traditional theory, developed from measurements using radioactive gases and chest wall scintillation counters, proposed that $\dot{V}_A/\dot{Q}$ matching is accomplished by gravity-mediated gradients of both ventilation and perfusion (19, 34, 35).

Experiments using higher resolution techniques in nonprimate species have demonstrated significantly greater heterogeneity of pulmonary perfusion than can be explained by gravitational mechanism alone (10, 14, 20, 25). Glenny et al. (10) estimated the maximal contribution of gravity to overall perfusion heterogeneity at ~7% in dogs. Recently, high-resolution measurements of regional perfusion in baboons (9) and indirect measurements of perfusion in humans under sustained microgravity conditions (24) suggested that nongravitational mechanisms of pulmonary perfusion distribution are also important in humans.

If gases are efficiently exchanged, regional perfusion heterogeneity has significant implications for regional ventilation. Wilson and Beck (36) mathematically demonstrated that, for a given heterogeneity of regional perfusion, as regional ventilation heterogeneity increases, the correlation between ventilation and perfusion must improve to preserve a narrow distribution of $\dot{V}_A/\dot{Q}$ values. Recent high-resolution measurements using either aerosolized 0.005-μm ^{99m}Tc-labeled carbon particles (18) or aerosolized 1-μm fluorescent microspheres (1, 26) demonstrated that regional ventilation is heterogeneous and highly correlated with local perfusion. Although mechanisms of ventilation heterogeneity have not been well studied, nitrogen washout experiments during space shuttle flights demonstrated persistent ventilation heterogeneity during microgravity, confirming the importance of nongravitational mechanisms on regional ventilation distribution (13, 23).

Close correlation between regional ventilation and perfusion suggests that regional ventilation has spatial characteristics similar to regional perfusion. One method used to characterize regional ventilation and perfusion distributions is fractal analysis. The incentive for applying fractal analysis in the study of perfusion or ventilation heterogeneity is that the observed heterogeneity of either measure is complicated by dependence on the scale of resolution. With the use of fractal analysis, this problem is resolved because the scale-dependent variability is described by a scale-independent fractal dimension. Fractal analysis is useful for several other reasons. A fractal pattern in ventilation heterogeneity implies the presence of spatial clustering in which ventilation to a given region is correlated with that of neighboring regions (12); this, in turn, can give insight into the mechanisms of regional ventilation distribution. Glenny (8) suggested that spatial clustering of regional blood flow supports the hypothesis that regional perfusion is determined by resistive differences in the branching pulmonary vascular tree (3). Fractal analysis may also be useful for identifying the anatomic level at which gas exchange is determined. Ventilation heterogeneity is unlikely to continue increasing as resolution improves because of forces that promote mixing, such as gas diffusion, reinspiration of common dead space gas, and cardiogenic oscillations. At some regional volume, alveolar gas tensions will become uniform, despite any perfusion heterogeneity. The volume of this region, termed the

The costs of publication of this article were defrayed in part by the payment of page charges. The article must therefore be hereby marked "*advertisement*" in accordance with 18 U.S.C. Section 1734 solely to indicate this fact.

 8750-7587/00 $5.00 Copyright © 2000 the American Physiological Society

unit of gas exchange, would be identified by a change in the slope of the fractal ventilation plot (Fig. 1). Finally, the scale-independent fractal dimension (*D*) provides a way to compare measurements of regional ventilation by using different techniques with varying resolutions.

To determine whether regional ventilation has fractal properties similar to regional perfusion, we measured ventilation and perfusion with aerosolized and injected microspheres in six juvenile pigs. To determine if posture had similar effects on regional ventilation and perfusion, measurements were taken in supine and prone postures.

METHODS

Animal preparation. The Animal Care Committee at the University of Washington approved these experiments. Six pigs, of either gender, weighing 18.5–25 kg, were studied. Anesthesia was introduced intramuscularly with ketamine and xylazine and followed by continuous intravenous thiopental sodium, at a rate sufficient to suppress spontaneous respiration. The animals were mechanically ventilated via tracheostomy with a tidal volume of ~15 ml/kg and a respiratory rate sufficient to maintain an arterial carbon dioxide tension between 30 and 40 Torr. One carotid and one femoral artery were cannulated for continuous blood pressure monitoring and withdrawal of blood samples. Two femoral veins were cannulated for administration of anesthesia and injection of microspheres. A pulmonary artery catheter was inserted through an external jugular vein. A standard solution of six inert gases was infused, but resultant data were not used for this analysis.

Study protocol. All animals were hyperinflated to twice the tidal volume every 10 min and before all measurements to minimize atelectasis. Data were collected twice in the prone posture and twice in the supine posture for each animal. Posture order was randomized for each experiment. Data collections were carried out at 30-min intervals, with posture change occurring at the beginning of the interval. Each data collection included measurement of mean arterial pressure, pulmonary artery pressure, peak airway pressure, temperature, hematocrit, the average of three thermodilution cardiac output measurements, and blood gas determined from arterial and mixed venous samples. After each data collection, aerosolized 1-μm fluorescent microspheres (FluoSpheres, Molecular Probes, Eugene, OR) were delivered over 10 min to measure regional ventilation as previously described (26). Simultaneously, 15-μm fluorescent microspheres (FluoSpheres, Molecular Probes) were injected intravenously in multiple, small, evenly spaced increments to measure regional perfusion. One regional ventilation measurement and one regional perfusion measurement were randomly chosen for simultaneous duplicate measurement in each experiment. A total of 10 different fluorescent labels were used (1-μm microspheres: yellow-green, yellow, orange, orange-red, red; 15-μm microspheres: blue, blue-green, green, crimson, scarlet). The fluorescent-label orders for both ventilation and perfusion markers were independently randomized before each experiment. After the last data collection, 10,000 units of heparin and 1.5 ml of papaverine were intravenously injected, and the animal was killed by exsanguination under deep anesthesia.

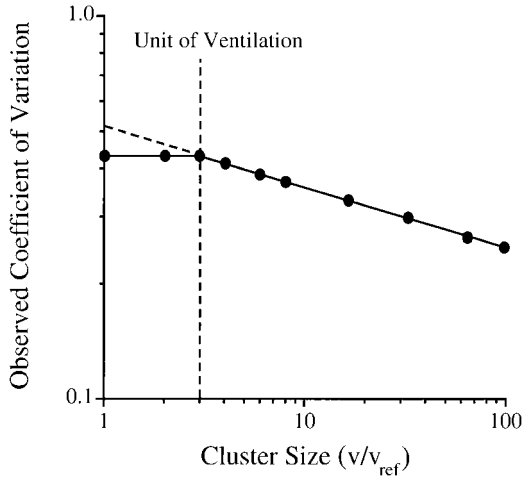

Fig. 1. A theoretical fractal plot of ventilation demonstrates no further increase in heterogeneity below a region size of 3 times the highest resolution. At this point, termed the unit of ventilation, uniformity of alveolar gas composition fixes gas exchange despite any further increases in perfusion heterogeneity. If the fractal plot continued to increase as depicted by the dashed line, then the unit of ventilation is below the obtained resolution. V/V_{ref}, ventilation at a regional volume/ventilation at smallest regional volume.

Lung preparation and data collection. A sternotomy was performed, the main pulmonary artery and left atrium were cannulated, and the aorta was ligated. The pulmonary vasculature was flushed with a dextran solution, and the lungs and trachea were dissected from the chest cavity and dried, inflated at 25-cmH_2O pressure.

The dried lungs were fixed in a rapid-setting foam, sliced, mapped, and diced into cubes of 1.5- to 2.0-cm^3 volume. Each piece was weighed, visually scored for airway and blood content, and soaked for 4 days in 2-ethoxyethyl acetate to extract the fluorescent dyes. Fluorescent signals for the 10 colors were measured in each piece with a fluorometer (LS50B, Perkin-Elmer, Beaconsfield, Buckinghamshire, UK). Spillover signals from colors adjacent in the spectrum were corrected by using matrix inversion of fixed wavelength intensities (28). Fluorescent signals were converted to number of microspheres by using the fluorescent intensity of reference samples containing a known number of microspheres. Pieces with airway content ≥25% of total piece volume were excluded from further analysis. Signals for each piece were normalized to that piece's weight, correcting for heterogeneity in ventilation and perfusion due to variation in piece size. The number of microspheres of each color in each piece was normalized to the mean number of microspheres of that color in all pieces, correcting for variations in the total number of microspheres of each given color.

Noise estimation. Observed heterogeneity of injected or aerosolized microsphere deposition consists of both true heterogeneity of regional ventilation or perfusion and heterogeneity introduced by methodological error. Methodological error for measurement of regional blood flow by injected microspheres approximates a Poisson distribution; therefore, the standard deviation of multiple simultaneous measurements will equal the square root of the mean measurement ($\overline{X}$) (2, 4, 38). Therefore, the coefficient of variation (CV, where $CV = SD/\overline{X}$) for simultaneous measurements will equal $1/\sqrt{\overline{X}}$. To evaluate the significance of methodological noise for measurement of regional ventilation by using aerosolized microspheres, four colors were simultaneously given to two animals over a 15-min period. In each animal, Pearson correlation coefficients (*r*) were calculated between each color and the mean of the other three colors. The CV of the four measurements of regional ventilation was plotted against $\overline{X}$ in that piece to determine if methodological variation approximated a Poisson distribution.

Fractal analysis and statistics. The same method of fractal analysis is applied to characterize both regional ventilation and perfusion; therefore, for simplicity, all further discussion of the method will implicitly apply to perfusion as well as ventilation. Heterogeneity of regional ventilation can be characterized by the CV. Given a Poisson distribution of methodological noise, the true CV (CV_{true}) is estimated from the observed CV (CV_{obs}) by

$$CV_{true} = \sqrt{\frac{CV_{obs}^2 - \left(\frac{n-1}{n}\right)\cdot\frac{1}{\overline{X}}}{1 - \frac{1}{n\cdot\overline{X}}}} \qquad (1)$$

where n is the number of pieces in which ventilation is measured and $\overline{X}$ is the mean number of microspheres per region (22). When n is large, this equation simplifies to the more familiar equation

$$CV_{true} = \sqrt{CV_{obs}^2 - \frac{1}{\overline{X}}} \qquad (2)$$

D is calculated from measurements of CV using the equation

$$CV(v) = CV(v_{ref})\cdot\left(\frac{v}{v_{ref}}\right)^{1-D} \qquad (3)$$

where CV(υ) is the CV of ventilation at a regional volume and $CV(\upsilon_{ref})$ is the CV of ventilation at the smallest regional volume examined in this study (~2 cm^3). The logarithm of both sides of *Eq. 2* describes a linear relationship with a slope of $1 - D$

$$\log CV(v) = (1 - D)\cdot\log\left(\frac{v}{v_{ref}}\right) + \log CV(v_{ref}) \qquad (4)$$

Therefore, D can be calculated from a linear least squares regression of a log-log plot of CV vs. υ/υ_{ref}.

We initially calculated the CV for a distribution of regional ventilation measured at a resolution of ~2 cm^3. Estimates of CV for ventilation distributions measured at larger regional volumes were calculated by randomly choosing a starting piece and then combining its ventilation with the ventilation of adjacent 2-cm^3 pieces. The software performing these calculations was constrained as follows: *1*) for each cluster size, the software formed as many clusters as possible without including any 2-cm^3 piece from more than one cluster, and *2*) clusters cannot contain pieces from more than one lobe. These constraints resulted in fewer ventilation measurements at larger cluster sizes. Therefore, the software repeated the calculations, starting with a new 2-cm^3 piece for cluster sizes greater than three pieces. This allowed calculation of a mean CV and standard error. A weighted linear regression algorithm was used to calculate the slope of the fractal plot. The total number of measurements used to calculate a CV at a given cluster size was used as a weighting factor for the linear regression calculation. For example, at the highest resolution, the CV of ventilation may be calculated from 1,000 measurements and is therefore weighted by 1,000. At a cluster size of eight pieces, the CV may be calculated from three repetitions of the clustering algorithm, each using an average of 109 ventilation measurements; therefore, 3 × 109 or 327 would weight that CV. Because of the constraints of the clustering software, increasing numbers of 2-cm^3 pieces were excluded from the CV calculation of larger cluster sizes, resulting in decreased confidence in the accuracy of the CV and a corresponding decreased weighting in the linear regression calculation.

Measurements of regional ventilation and perfusion were taken twice in both the supine and prone postures. To look at the interanimal variability of ventilation and perfusion heterogeneity, a mean value for each posture was calculated for CV and D of both ventilation and perfusion in each animal. All values are presented as mean ± SD. Paired *t*-tests were used for statistical comparisons, with $P < 0.05$ considered a significant difference.

RESULTS

Physiological response. Tidal volumes and respiratory rates, once set, remained constant throughout the experiment, except for the second animal, in which respiratory rate was decreased after the second set of measurements to correct for respiratory alkalosis. There was no significant difference between prone and supine postures for airway, mean arterial, and mean pulmonary artery pressures. There was a trend toward a lower cardiac output in the supine posture, by a mean of 215 ml/min, but this did not reach statistical significance ($P = 0.063$). The average alveolar-arterial oxygen tension was significantly greater in the supine posture compared with the prone posture (mean difference = 7.38 Torr, $P = 0.028$).

Methodological noise estimate. Two animals were studied to estimate the contribution of methodological noise to the observed heterogeneity of ventilation. In the second animal studied, the last 100 samples had significant degradation of yellow-green intensity, likely attributable to exposure to a heat source. These 100 samples were excluded from the analysis, leaving 715 pieces. All 954 pieces of the first animal's lung were included in analysis. In both animals, the total number of microspheres administered varied from color to color due to imprecision in the administration of the quantities of aerosols. We compensated for this difference by averaging the total number of microspheres deposited between colors and normalizing the number of microspheres in each piece to this value. Correlations between a specific color and the mean of the other three colors are given in Table 1 and averaged 0.995 ± 0.002. In both animals, the CV of regional deposition of four simultaneously administered aerosols decreased as a power function of the mean number of regional microspheres (Fig. 2), with an average exponent of − 0.51 ± 0.11.

Table 1. *Correlation coefficients between each color and the mean of the 3 remaining colors after simultaneous administration of 4 aerosol colors*

	r			
Animal	$Color_1$/Mean	$Color_2$/Mean	$Color_3$/Mean	$Color_4$/Mean
1	0.993	0.995	0.995	0.997
2	0.990	0.996	0.994	0.997
Mean	0.992	0.996	0.995	0.997

r, Pearson correlation coefficient; Color/Mean, color-to-mean ratio; subscripts, color number.

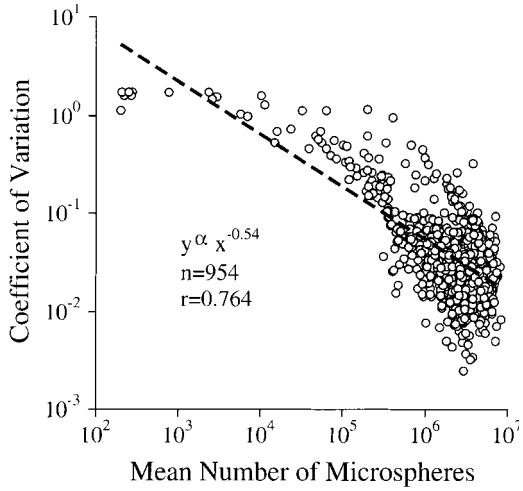

Fig. 2. The coefficients of variation of 4 simultaneously administered aerosols is proportional to the inverse square root of the mean number of microspheres. This suggests that a Poisson distribution may describe a portion of the method error for aerosol measurement of regional ventilation. *n*, Number of samples.

Fractal analysis. The CV for both ventilation and perfusion at the smallest region size are shown in Table 2. There is no significant difference between CV for ventilation and perfusion in either posture, despite the wide range of CV observed between animals. CV is significantly greater in the supine posture compared with the prone posture for both ventilation (mean difference = 0.065; $P = 0.04$) and perfusion (mean difference = 0.105; $P = 0.02$). Despite the high degree of observed heterogeneity in regional ventilation and perfusion, a narrow distribution of $\dot{V}_A/\dot{Q}$ is preserved through close correlation between regional ventilation and perfusion (Table 3).

Equation 4 provides a reasonable fit of observed heterogeneity for regional ventilation and perfusion as a function of region size (Fig. 3). The average coefficients of determination (r^2) for ventilation fractal plots in the prone and supine postures are 0.80 ± 0.06 and 0.63 ± 0.18, respectively. The average r^2 for perfusion fractal plots in the prone and supine postures are 0.84 ± 0.06 and 0.80 ± 0.04, respectively. At clusters $\geq 32 \times \upsilon_{ref}$, the standard deviation of the CV measurement increases significantly, and the data are not as well described by *Eq. 4*. Because of the constraint that all pieces in a cluster be within the same lobe, it is difficult to form more than a few clusters at sizes $\geq 32 \times \upsilon_{ref}$. Given the finite ventilation or perfusion to a given lung, flow will be negatively correlated between large clusters, resulting in a poor fit to the linear model at the largest cluster sizes (clusters $> 32 \times n$ in animals of this size). This poor fit of the largest clusters to the fractal model has minimal effect on the calculation of *D* because the linear regression is weighted by the number of measurements used to calculate CV at each resolution.

Table 2. *Observed coefficients of variation for perfusion and ventilation in the prone and supine postures at the highest resolution*

	CV of Ventilation		CV of Perfusion	
Animal	Prone	Supine	Prone	Supine
1	0.51	0.61	0.50	0.65
2	0.38	0.40	0.45	0.50
3	0.62	0.61	0.70	0.72
4	0.47	0.58	0.50	0.58
5	0.65	0.69	0.55	0.66
6	0.47	0.60	0.42	0.64
Mean ± SD	0.52 ± 0.10	0.58 ± 0.10	0.52 ± 0.10	0.63 ± 0.08

CV, coefficient of variation.

Table 3. *$\dot{V}_A/\dot{Q}$ matching is preserved by close correlation of regional ventilation and perfusion in prone and supine positions*

	SD, $\dot{V}_A/\dot{Q}$		*r*, $\dot{V}_A/\dot{Q}$	
Animal	Prone	Supine	Prone	Supine
1	0.474	0.791	0.871	0.746
2	0.490	0.821	0.769	0.622
3	0.645	0.845	0.857	0.752
4	0.569	0.742	0.725	0.731
5	0.750	1.066	0.821	0.742
6	0.515	0.849	0.788	0.727
Mean ± SD	0.574 ± 0.106	0.852 ± 0.112	0.805 ± 0.055	0.720 ± 0.049

$\dot{V}_A/\dot{Q}$, ventilation-to-perfusion ratio.

The *D* for individual animals is shown in Table 4. The *D* of ventilation is less than that of perfusion in the prone posture, by a mean difference of 0.035 ($P = 0.016$). In the supine posture, the mean difference between the ventilation and perfusion *D* increases to 0.057 ($P = 0.0001$). The *D* in the supine posture is lower than in the prone posture for both ventilation (mean difference = 0.066, $P = 0.003$) and perfusion (mean difference = 0.044, $P = 0.035$).

DISCUSSION

This study uses aerosolized deposition of fluorescently labeled microspheres to measure regional ventilation with resolution similar to that of regional perfu-

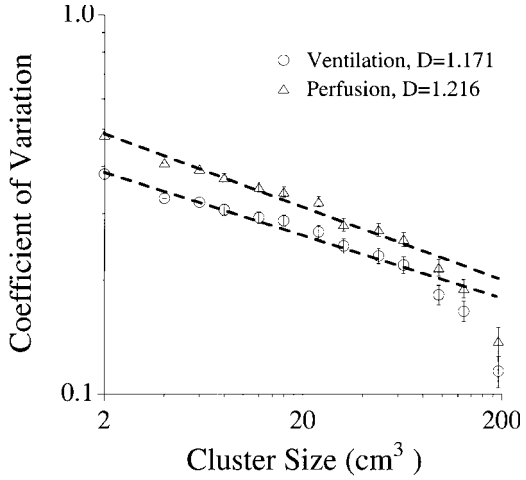

Fig. 3. Regression lines of a fractal (log-log) plot fit the data well for both ventilation and perfusion. No leveling of the plot for ventilation is noted, indicating that the unit of ventilation is below the current resolution (~2 cm^3). *D*, fractal dimension.

Table 4. *Fractal dimensions for ventilation and perfusion in the prone and supine postures*

	D of Ventilation		*D* of Perfusion	
Animal	Prone	Supine	Prone	Supine
1	1.159	1.109	1.188	1.152
2	1.171	1.115	1.216	1.179
3	1.184	1.074	1.210	1.150
4	1.197	1.147	1.256	1.208
5	1.081	1.047	1.075	1.092
6	1.152	1.057	1.207	1.108
Mean ± SD	1.157 ± 0.041	1.092 ± 0.038	1.192 ± 0.061	1.148 ± 0.043

D, fractal dimension.

sion measurements. With the use of a clustering algorithm, the fractal characteristics of ventilation are examined in a fashion analogous to that applied to regional perfusion. The important findings from this study are that *1*) regional ventilation and perfusion are similarly heterogeneous, but closely correlated, permitting efficient gas exchange; *2*) regional ventilation and perfusion have similar fractal characteristics; *3*) the *D* of both ventilation and perfusion is lower in the supine posture than in the prone posture; and *4*) the error of measuring regional ventilation is small and partially explained by a Poisson distribution.

Implications for gas exchange. Wilson and Beck (36) have mathematically shown that $\dot{V}_A/\dot{Q}$ heterogeneity and gas exchange are determined by the heterogeneity of regional perfusion, regional ventilation, and the correlation between ventilation and perfusion. This study demonstrates that, as the resolution of regional ventilation and perfusion measurement improves, the observed heterogeneity of both ventilation and perfusion increases. Despite this heterogeneity, a narrow distribution of $\dot{V}_A/\dot{Q}$ is preserved through close correlation of regional ventilation and perfusion (Fig. 4). Because both observed perfusion heterogeneity (11) and variability of parenchymal expansion (27) increase at resolutions greater than those obtained in this study, gas exchange efficiency is likely determined by the degree of regional correlation between ventilation and perfusion at volumes <2 cm^3. At some level, mixing of alveolar gas by diffusion and reinspiration of common dead space will result in a homogeneous gas composition and uniform end-capillary oxygen contents within the volume of ventilation. Experiments measuring the change in physiological dead space after graded embolization suggest that homogeneous gas exchange occurs at the level of the acinus (37). However, modeling of nitrogen washouts within an acinus suggests that heterogeneity of regional gas composition is present at a subacinar level (7).

Implications for ventilation distribution. A fractal pattern of ventilation heterogeneity implies that regional ventilation has spatial clustering characteristics similar to those of regional perfusion (Fig. 5) (12). This spatial pattern of regional ventilation promotes speculation regarding mechanisms that determine regional ventilation. Recent theoretical work by West et al. (32, 33) shows that fractal distribution of a substrate explains the 1/4 allometric scaling law observed throughout nature. Their model, based, in part, on the assumption that the energy required to distribute a substrate throughout a region must be minimized for maximal efficiency, predicts observed allometric exponents relating lung structure and function to body mass. Fractal regional ventilation must be determined by regional heterogeneity of lung structure. Given the fractal structure of the bronchial tree (17, 31), it is tempting to attribute regional ventilation heterogeneity primarily to differences in regional airway impedance. Studies using both modeling and measurement of alveolar pressure demonstrate that tissue impedance comprises a significant component of total lung impedance at normal ventilation frequencies and is responsible for almost all of the frequency dependence of lung impedance (15, 16, 21). This would suggest that regional ventilation distribution is primarily determined by regional tissue impedance; however, these methods do not give adequate spatial information to draw this conclusion. Despite tissue impedance being greater than airway impedance, if tissue impedance is uniformly distributed, then airway structure may still be the principal determinant of regional ventilation heterogeneity.

Implications of posture effect on D. The *D* of both perfusion and ventilation is lower in the supine posture compared with the prone posture. The significance of this is that spatial correlation must be greater for both ventilation and perfusion in the supine posture. This likely represents the superimposition of an organizing influence on the innate heterogeneity caused by pulmonary structure. Likely candidates for this effect are a hydrostatic gradient for pulmonary perfusion (35) and a topographically distributed change in compliance for ventilation (19). These mechanisms resulted in only a small increase in heterogeneity of both ventilation and perfusion (Table 1); however, the effects on ventilation and perfusion are apparently not spatially matched, resulting in increased $\dot{V}_A/\dot{Q}$ mismatch and, therefore,

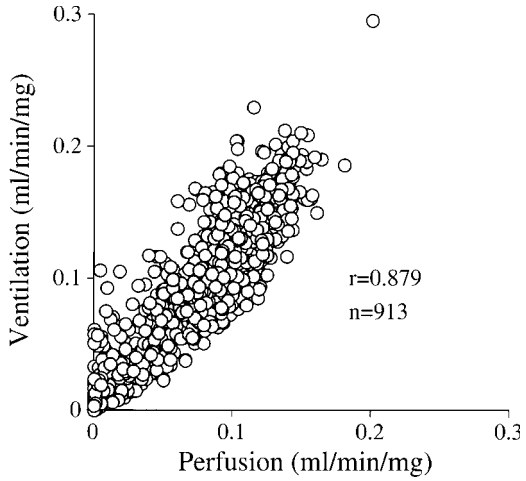

Fig. 4. Regionally heterogeneous ventilation and perfusion are spatially correlated, preserving a narrow ventilation-to-perfusion distribution ratio ($\dot{V}_A/\dot{Q}$) and efficient gas exchange.

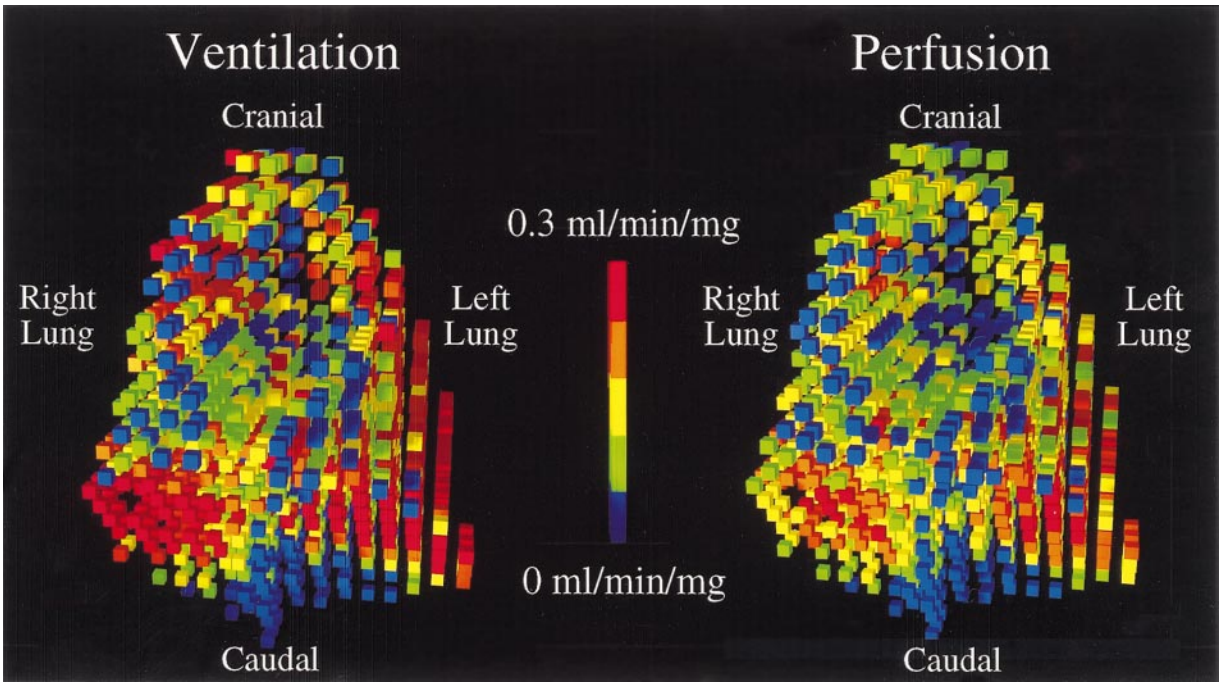

Fig. 5. Regional ventilation and perfusion scaled to the measured minute ventilation and cardiac output. Both ventilation and perfusion display regional clustering in which adjacent regions have similar flows. Note the strong spatial correlation where regions that receive high ventilation receive high perfusion and regions that receive less ventilation receive less perfusion.

the increased alveolar-arterial oxygen difference observed in the supine posture.

Contribution of method error to regional heterogeneity measurement. The aerosolized microsphere method has minimal noise and good reproducibility, as demonstrated by the high correlations between simultaneously aerosolized microspheres. The CV of simultaneously aerosolized microspheres decreases in proportion to the inverse square root of $\overline{X}$, suggesting that a Poisson distribution describes a portion of the method error. The aerosol concentration of individual colors was two to four times greater in the fractal experiments than in the experiments estimating method error. Hence, the contribution of method error to our measurements is small at measurement resolution. Method error decreases as regional volume increases (resolution decreases) because of increasing regional microsphere deposition.

In conclusion, efficient gas exchange is dependent on the close matching of regional ventilation and perfusion. Given the high degree of heterogeneity observed at small regional volumes in this study, ventilation and perfusion must be closely correlated to achieve this matching. In the normal lung, this must occur by one of the following three mechanisms: *1*) active matching of regional perfusion to ventilation, *2*) active matching of regional ventilation to perfusion, or *3*) passive matching of ventilation and perfusion by innate pulmonary structure. In the normal lung, basal pulmonary vascular tone is minimal, suggesting that vasoregulation is of minor importance for maintaining close $\dot{V}_A/\dot{Q}$ matching in uninjured lungs (5, 6, 29, 30). In pigs, there is minimal ventilation redistribution after regional perfusion changes from microembolism, suggesting that active regulation of ventilation distribution is minimal (1). Passive matching of ventilation and perfusion by pulmonary structure is appealing because it requires the least amount of energy. An optimally engineered system requires no active feedback mechanisms during normal function. Pathological conditions, however, may require feedback mechanisms to correct instabilities. Regional ventilation and blood flow are both distributed through fractal structures that share similar geometry. It is tempting to assign responsibility for the fractal distribution patterns of ventilation and blood flow to the bronchial and pulmonary arterial trees, respectively. The high correlation between regional ventilation and perfusion that permits efficient gas exchange, despite high spatial heterogeneity, may be explained by the close correlation of the developing bronchial tree and pulmonary arterial tree during organogenesis, as first suggested by Weibel (31). Fractal distribution networks for ventilation and perfusion provide several inherent advantages. Fractal structures are the most efficient way to fill a three-dimensional structure and provide the most energy efficient substrate transport (33). A fundamental characteristic of a fractal structure is that its basic form is replicated over a range of scales. This repetition would permit efficient genetic coding. The fractal nature of heterogeneity, as measured by our analysis, does not prove that regional ventilation and pulmonary perfusion distribution are determined by fractal pulmonary structure, but it is supportive of this idea. Further investigation into the determinants of regional ventilation and the matching between ventilation and perfu-

sion is necessary to fully understand the gas exchange function of the lung.

We thank Dowon An and Shen-Sheng Wang for technical assistance and Dave Frazer for assistance with figure preparation.

This work was supported by National Heart, Lung, and Blood Institute Grant HL-10003 and by an American Lung Association Washington State Affiliate Research Grant.

Address for reprint requests and other correspondence: W. A. Altemeier, Div. of Pulmonary and Critical Care Medicine, BB-1253 Health Sciences Building, Box 356522, Seattle, Washington 98195-6522 (E-mail: billa@u.washington.edu).

Received 23 September 1999; accepted in final form 14 December 1999.

REFERENCES

1. **Altemeier WA, Robertson HT, McKinney S, and Glenny RW.** Pulmonary embolization causes hypoxemia by redistributing regional blood flow without changing ventilation. *J Appl Physiol* 85: 2337–2343, 1998.
2. **Austin, RE Jr, Hauck WW, Aldea GS, Flynn AE, Coggins DL, and Hoffman JI.** Quantitating error in blood flow measurements with radioactive microspheres. *Am J Physiol Heart Circ Physiol* 257: H280–H288, 1989.
3. **Beck KC and Rehder K.** Differences in regional vascular conductances in isolated dog lungs. *J Appl Physiol* 61: 530–538, 1986.
4. **Buckberg GD, Luck JC, Payne DB, Hoffman JI, Archie JP, and Fixler DE.** Some sources of error in measuring regional blood flow with radioactive microspheres. *J Appl Physiol* 31: 598–604, 1971.
5. **Celermajer DS, Dollery C, Burch M, and Deanfield JE.** Role of endothelium in the maintenance of low pulmonary vascular tone in normal children. *Circulation* 89: 2041–2044, 1994.
6. **Cooper CJ, Landzberg MJ, Anderson TJ, Charbonneau F, Creager MA, Ganz P, and Selwyn AP.** Role of nitric oxide in the local regulation of pulmonary vascular resistance in humans. *Circulation* 93: 266–271, 1996.
7. **Engel LA.** Gas mixing within the acinus of the lung. *J Appl Physiol* 54: 609–618, 1983.
8. **Glenny RW.** Spatial correlation of regional pulmonary perfusion. *J Appl Physiol* 72: 2378–2386, 1992.
9. **Glenny RW, Bernard S, Robertson HT, and Hlastala MP.** Gravity is an important but secondary determinant of regional pulmonary blood flow in upright primates. *J Appl Physiol* 86: 623–632, 1999.
10. **Glenny RW, Lamm WJ, Albert RK, and Robertson HT.** Gravity is a minor determinant of pulmonary blood flow distribution. *J Appl Physiol* 71: 620–629, 1991.
11. **Glenny RW and Robertson HT.** Fractal properties of pulmonary blood flow: characterization of spatial heterogeneity. *J Appl Physiol* 69: 532–545, 1990.
12. **Glenny RW, Robertson HT, Yamashiro S, and Bassingthwaighte JB.** Applications of fractal analysis to physiology. *J Appl Physiol* 70: 2351–2367, 1991.
13. **Guy HJ, Prisk GK, Elliot AR, Deutschman RA III, and West JB.** Inhomogeneity of pulmonary ventilation during sustained microgravity as determined by single-breath washouts. *J Appl Physiol* 76: 1719–1729, 1994.
14. **Hlastala MP, Bernard SL, Erickson HH, Fedde MR, Gaughan EM, McMurphy R, Emery MJ, Polissar N, and Glenny RW.** Pulmonary blood flow distribution in standing horses is not dominated by gravity. *J Appl Physiol* 81: 1051–1061, 1996.
15. **Ludwig MS, Dreshaj I, Solway J, Munoz A, and Ingram RH Jr.** Partitioning of pulmonary resistance during constriction in the dog: effects of volume history. *J Appl Physiol* 62: 807–815, 1987.
16. **Lutchen KR, Greenstein JL, and Suki B.** How inhomogeneities and airway walls affect frequency dependence and separation of airway and tissue properties. *J Appl Physiol* 80: 1696–1707, 1996.
17. **Mandelbrot BB.** *The Fractal Geometry of Nature.* San Francisco, CA: Freeman, 1983.
18. **Melsom MN, Kramer-Johansen J, Flatebo T, Muller C, and Nicolaysen G.** Distribution of pulmonary ventilation and perfusion measured simultaneously in awake goats. *Acta Physiol Scand* 159: 199–208, 1997.
19. **Milic-Emili J, Henderson JA, Dolovich MB, Trop D, and Kaneko K.** Regional distribution of inspired gas in the lung. *J Appl Physiol* 21: 749–759, 1966.
20. **Nicolaysen G, Shepard J, Onizuka M, Tanita T, Hattner RS, and Staub NC.** No gravity-independent gradient of blood flow in dog lung. *J Appl Physiol* 63: 540–545, 1987.
21. **Petak F, Hantos Z, Adamicza A, and Daroczy B.** Partitioning of pulmonary impedance: modeling vs. alveolar capsule approach. *J Appl Physiol* 75: 513–521, 1993.
22. **Polissar NL, Stanford DC, and Glenny RW.** The 400 microsphere per piece "rule" does not apply to all blood flow studies. *Am J Physiol Heart Circ Physiol* 278: H16–H25, 2000.
23. **Prisk GK, Guy HJ, Elliott AR, Paiva M, and West JB.** Ventilatory inhomogeneity determined from multiple-breath washouts during sustained microgravity on Spacelab SLS-1. *J Appl Physiol* 78: 597–607, 1995.
24. **Prisk GK, Guy HJ, Elliot AR, and West JB.** Inhomogeneity of pulmonary perfusion during sustained microgravity on SLS-1. *J Appl Physiol* 76: 1730–1738, 1994.
25. **Reed JH and Wood EH.** Effect of body position on vertical distribution of pulmonary blood flow. *J Appl Physiol* 28: 303–311, 1970.
26. **Robertson HT, Glenny RW, Stanford D, McInnes LM, Luchtel DL, and Covert D.** High-resolution maps of regional ventilation utilizing inhaled fluorescent microspheres. *J Appl Physiol* 82: 943–953, 1997.
27. **Rodarte JR, Chaniotakis M, and Wilson TA.** Variability of parenchymal expansion measured by computed tomography. *J Appl Physiol* 67: 226–231, 1989.
28. **Schimmel C, Frazer D, and Glenny R.** Curve fitting and matrix inversion enables the use of 10 colors for measuring regional organ blood flow with fluorescent microspheres. *Exp Biol* 12: part II, 1998.
29. **Stamler JS, Loh E, Roddy MA, Currie KE, and Creager MA.** Nitric oxide regulates basal systemic and pulmonary vascular resistance in healthy humans. *Circulation* 89: 2035–2040, 1994.
30. **Uncles DR, Daugherty MO, Frank DU, Roos CM, and Rich GF.** Nitric oxide modulation of pulmonary vascular resistance is red blood cell dependent in isolated rat lungs. *Anesth Analg* 83: 1212–1217, 1996.
31. **Weibel ER.** Fractal geometry: a design principle for living organisms. *Am J Physiol Lung Cell Mol Physiol* 261: L361–L369, 1991.
32. **West GB, Brown JH, and Enquist BJ.** A general model for the origin of allometric scaling laws in biology. *Science* 276: 122–126, 1997.
33. **West GB, Brown JH, and Enquist BJ.** The fourth dimension of life: fractal geometry and allometric scaling of organisms. *Science* 284: 1677–1679, 1999.
34. **West JB.** Regional differences in gas exchange in the lung of erect man. *J Appl Physiol* 17: 893–898, 1962.
35. **West JB, Dollery CT, and Naimark A.** Distribution of blood flow in isolated lung: relation to vascular and alveolar pressures. *J Appl Physiol* 19: 713–724, 1964.
36. **Wilson TA and Beck KC.** Contributions of ventilation and perfusion inhomogeneities to the $\dot{V}_A/\dot{Q}$ distribution. *J Appl Physiol* 72: 2298–2304, 1992.
37. **Young I, Mazzone RW, and Wagner PD.** Identification of functional lung unit by graded vascular embolization. *J Appl Physiol* 49: 132–141, 1980.
38. **Zwissler B, Schosser R, Weiss C, Iber V, Weiss M, Schwickert C, Spengler P, and Messmer K.** Methodological error and spatial variability of organ blood flow measurements using radiolabeled microspheres. *Res Exp Med (Berl)* 191: 47–63, 1991.